IV.A.5 Reversible Hydrogen Storage Materials – Structure, Chemistry, and Electronic Structure

Ian M. Robertson (Primary Contact) and
Duane D. Johnson
University of Illinois at Urbana-Champaign (UIUC)
Department of Materials Science and Engineering
1304 West Green Street
Urbana, IL 61801
Phone: (217) 333-6776
E-mail: ianr@illinois.edu

DOE Managers
HQ: Ned Stetson
Phone: (202) 586-9995
E-mail: Ned.Stetson@ee.doe.gov
GO: Paul Bakke
Phone: (720) 356-1436
E-mail: Paul.Bakke@go.doe.gov

Contract Number: DE FC36-05GO15064

Project Start Date: March 1, 2005
Project End Date: February 26, 2011

Objectives

The main focus of this research project is to:

- Advance the understanding of the microstructural and modeling characteristics of complex hydrides.
- Provide more reliable theoretical methods to assess hydrogen-storage materials, including key issues affecting materials under study.

Technical Barriers

This project addresses the following technical barriers from the Fuel Cell Technologies Program Multi-Year Research, Development and Demonstration Plan:

(A) System Weight and Volume
(E) Charging/Discharging Rates
(D) Durability/Operability

Technical Targets

This project is conducting fundamental experimental and theoretical studies of candidate light-weight systems for on-board regeneration. Insights gained from these studies will be applied toward the design and synthesis of hydrogen storage materials that meet the following DOE 2010 hydrogen storage targets:

- Cost: $4/kWh net
- Specific energy: 1.5 kWh/kg
- Energy density: 0.9 kWh/L

Introduction

The effort at the University of Illinois at Urbana-Champaign focuses on resolving issues within current hydrogen storage materials using a combination of electronic structure calculations and state-of-the-art compositional and structural characterization methods. We tie together theoretical understanding of electronic, enthalpic, thermodynamic, and surface effects affecting performance of storage materials with microcompositional and microstructural experimental analysis, coordinated with collaborative partnerships with other institutions; current partnerships are with Savannah River National Laboratory, Dr. Ragaiy Zidan, and University of Missouri, Professor Eric Majzoub. These efforts enable a more efficient approach to designing a new system with the required properties.

Approach

We employ state-of-the-art characterization tools to investigate the microstructural and microchemical changes that occur in candidate material systems during the uptake and release of hydrogen. The characterization is coupled with first-principles, electronic-structure and thermodynamic theoretical techniques to predict and assess meta-stable and stable phases, as well as surface effects that can poison or limit kinetics. Electronic-structure and thermodynamic calculations are used to enhance the understanding of experimental characterization results on candidate systems. This combined theoretical/characterization effort provides fundamental insight to the processes governing hydrogen uptake and release. In the following, a selection of the highlights from the work performed in Fiscal Year 2011 is described.

Experimental Project

Our experimental effort utilizes the advanced characterization capabilities of a state-of-the art transmission electron microscope (TEM). An environmental transfer TEM stage enables air-sensitive materials to be loaded into the stage in the environment of a glove box and transferred to the microscope without exposure to the environment. In addition, electron tomography is being applied to gain three-dimensional information as to the particle shape, the distribution of catalyst particles dispersed by ball-milling

and the infiltration of the storage medium in nano-confined scaffolds. These approaches are being used to characterize air-sensitive nano-confined hydrogen storage materials to gain a better understanding of the effect of processing conditions on the resulting specimen structure and the effect of the number of cycles. Finally, scanning tunneling microscopy (STM) experiments are being conducted to identify the roadblock to hydrogen uptake and release in Al. The progress made this fiscal year is described in the following sections.

Nano-Porous Frameworks for Supporting Hydrogen Storage Materials

In collaboration with Professor Eric Majzoub and coworkers from the University of Missouri, we are investigating $LiBH_4$-infiltrated nano-porous carbon scaffolds. Existing work suggests that reducing the particle size of complex metal hydride materials (to 10 nm or smaller) enhances the kinetics and thermodynamics of hydrogen uptake and release. Infiltrating these materials into nano-porous scaffolds holds potential as a means for constraining particle size to the scaffold pore size as well as preventing the storage medium from sintering or its constituents from diffusing too far away.

The scaffolds we are examining were reported to be nano-porous carbon composed of long cylindrical columns packed into a hexagonal arrangement that run the entire length of the powder grains. The bright-field electron micrographs presented as Figures 1a and 1d are of the carbon scaffold and were reported to be representative of a side view and a pore-down view of the columns, respectively [1]. In these images, the columns (light) appear to be 2.1-2.5 nm wide with wall thicknesses (dark) of 9.1-9.8 nm and a column spacing of 13 nm. Similarly, pore diameters are 3-4.25 nm and the pore spacing is 14 nm. In contrast, we have shown that in both bright-field and high-angle annular dark-field scanning transmission electron images, Figures 1b-c and 1e-f, the column widths and wall thicknesses are identical (4-5 nm with a spacing between 8-9.5 nm) irrespective of the viewing direction and imaging mode. A second size of column, roughly half the width and half the spacing, is also seen though is less common. Still, the column diameters and wall thicknesses match each other. These new findings conform to the expected values based off other measurement techniques.

Our investigation has also revealed a number of interesting features about the scaffold structure, which are providing insight into the connection between processing conditions and how the scaffold grows. The columns form a layered structure, the sheets of columns of which are not always oriented in the same direction. Figure 1f shows one such particle in which the column layers are offset at hexagonal angles, giving incorrectly the appearance of pores. Other particles possess not only different orientations of columns but different sizes and curvatures of columns all within the same powder grain. Many particles are also

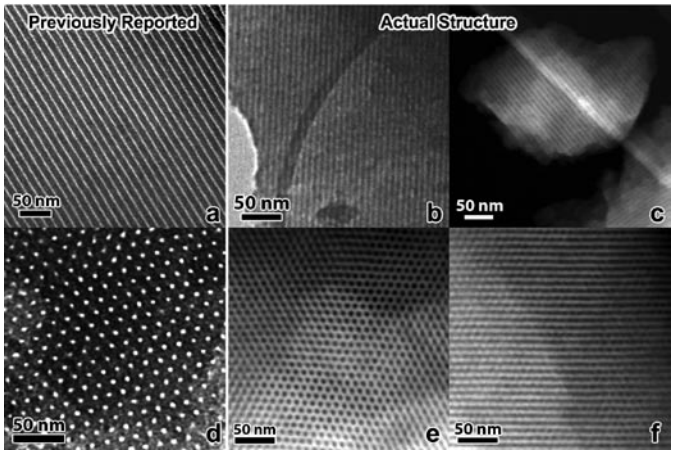

FIGURE 1. (a) Bright-field (BF) TEM micrograph from Mazjoub showing a large disparity between column width (light) and wall thickness (dark). (b) BF TEM micrograph taken at UIUC exhibiting no such disparity. (c) High-angle annular dark-field (HAADF) scanning transmission electron microscopy (STEM) micrograph taken at UIUC showing the same as (b). (d) BF TEM of pores again showing inaccurate structure. (e) HAADF STEM image from UIUC of pores and (f) layers of columns offset at hexagonal angles to give the appearance of pores.

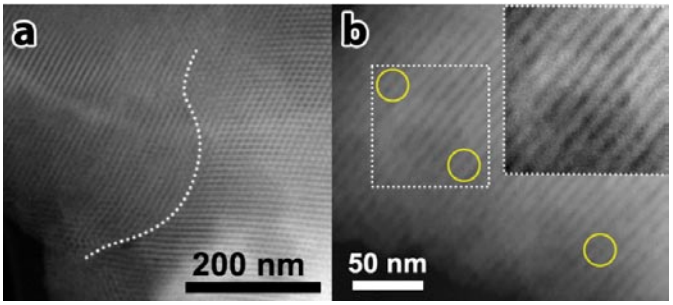

FIGURE 2. HAADF STEM micrographs showing (a) multiple domains of columns with different orientations within a scaffold particle (domain boundary shown by dotted line), and (b) column blockages (circled). The inset is a close-up of the boxed region, with the contrast adjusted for ease of viewing.

made of multiple domains of different column orientations, Figure 2a, the size and quantity of which may be a consequence of growth parameters. This domain structure might explain why the observed maximum practical loading capacity of these scaffolds is lower than would be expected according to scaffold volume. Any domains without pores directly open to the surface would be difficult or impossible to infiltrate fully. Similarly, column blockage has been observed, Figure 2b, and could also reduce the loading capacity. The extent of column blockage may be related to the concentration of oxygen flowed during synthesis. Further study of scaffold structures produced under a variety of processing conditions will elucidate their effect on the resulting microstructure, allowing optimal growth conditions to be determined.

In order to help understand and explain the gradual loss of total storage capacity observed with hydrogen cycling of

these systems [1], specimens that were desorbed at 500°C in a differential scanning calorimeter (DSC) were examined via electron microscopy. In these specimens, protruding material, in the form of bristles and nodules, were seen on the surfaces of the specimens. As shown in the images presented in Figure 3, the bristles were typically 16-24 nm wide with aspect ratios ranging from above 3:1 to over 6:1, though bristles down to around 13 nm and over 30 nm wide were observed. The nodules were usually many tens of nanometers in width and came in a variety of shapes. These bristles and nodules are not products of electron beam damage, as can sometimes be seen in bulk versions of these materials. Unlike the latter, these protrusions are present in their full form from the very beginning of observation and do not grow larger under continued exposure to the beam.

A possible explanation for these formations is that they are one or more components of the storage medium (Li and/or B) that migrates out from the carbon scaffold pores during hydrogen desorption, segregating to the scaffold particle surface where it grows into nodules and bristles. This reduces the amount of nano-scale infiltrated material available to participate in hydrogen uptake, lowering the total storage capacity of the system. Additionally, if the protrusions are composed of only either Li or B, this segregation of reaction components would also lead to a reduction in storage capacity, as would if the protrusions were a new stable, lower-reactivity compound. The low atomic mass of the storage medium (Li, B) makes chemical identification of the bristles and nodules quite difficult. In addition, the small size of the protrusions, as well as their composition, makes focused-probe methods impossible, as the bristles and nodules are immediately destroyed under such an intense electron beam. This behavior, though, strongly suggests that they are purely B and/or Li. We are currently investigating other techniques to find one that possesses the necessary resolution and chemical sensitivity, but will not destroy the protrusions.

The spatial density of surface bristles and nodules can vary dramatically across a single host scaffold particle. Some regions had densely packed patches of bristles while others were bare. It is possible that their distribution is related to where the column domains contact the surface.

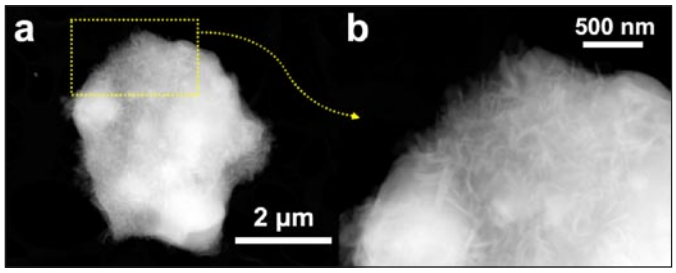

FIGURE 3. HAADF STEM images of a host scaffold particle covered in bristles and nodules. The area outlined in yellow in (a) is shown closer up in (b) to make the dense covering of bristles easier to see.

If the domain was oriented such that the column pores face the surface, it would be easier for the infiltrated storage material to migrate out of the pores and onto the surface to grow these protrusions.

The desorption temperature of these specimens (500°C) was higher than is used during standard cycling (300-350°C), so this behavior may be lessened or absent entirely under normal conditions. We are currently examining specimens of a variety of different filling ratios as they are heated from room temperature up to 500°C to determine the role of temperature in the formation of the bristles and nodules.

Preliminary studies, using a variable temperature scanning tunneling microscope, of clean Al surfaces and Al surfaces with sub-monolayer coverage of Ti, showed interesting results on the association of alane formation with the Ti atoms and with surface vacancies. Despite numerous attempts these results were difficult to reproduce. However, our recent first principle calculations, which are described in the following section, have provided insight as to the important role of surface defects. This insight suggests an alternate surface preparation strategy to the one used previously and another set of experiments has been initiated. New materials have been acquired, which we will use in our attempt to confirm our previous observations of Ti-catalyst activity on Al surfaces and the formation of alane with H_2 exposure.

Our latest experiments, using an STM with more sensitive spectroscopic capabilities to probe electronic structure, confirm that titanium catalyst deposited on an aluminum surface retains its metallic character; no energy gap is observed. Subsequent experiments will measure whether this changes with hydrogen exposure.

Theory

Transition-metal catalysts are used extensively in hydrogen storage materials to increase H absorption and desorption kinetics. Using density functional theory (DFT) calculations, we elucidated the catalytic effect of Ti substitution on H_2 desorption from a MgH_2(110) surface. Kinetic energy barriers of different reaction pathways of H desorption are calculated via the nudged-elastic-band (NEB) method. We found that a single Ti dopant is effective in reducing the kinetic barrier by 0.41 eV due to a concerted motion of H_2 surface desorption and H bulk diffusion. We also find that magnetic degrees of freedom must be carefully included to describe the crossover of magnetic states during catalyzed H_2 surface desorption. As shown in Figure 4, there are two concerted activation steps. In the early stage of reaction, the diffusion of in-plane hydrogen from first and second tri-layers to the surface brings a high hydrogen coordination number (HCN) of 8 to Ti, and the system prefers to have a magnetic moment of 0 μ_B. The activation barrier is small. In the second activation step to desorb H_2, the barrier is large. And importantly, because of the decrease in HCN to 6, the system prefers to have a magnetic

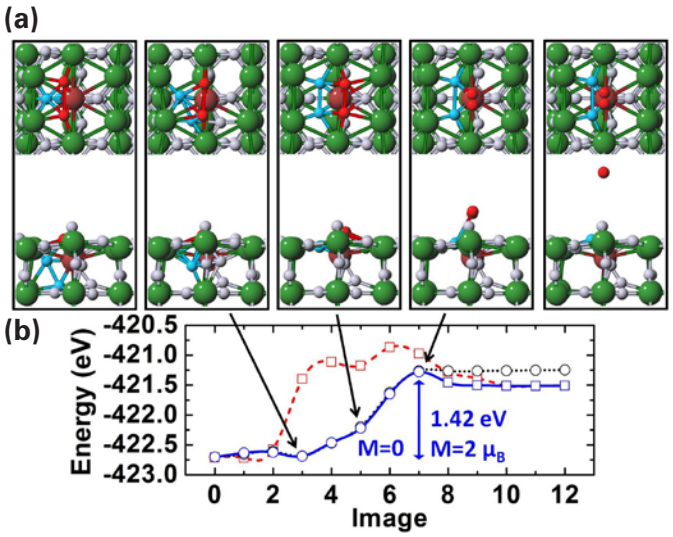

FIGURE 4. Minimum energy pathway (MEP) for H_2 desorption from Ti-doped MgH_2(110) surface, with large green spheres for Mg, large red for Ti and small gray for H. a) The leftmost (rightmost) sub-figure is the initial (final) state with a magnetic moment of 0 (2) μ_B. Three other intermediate states (Nudged elastic band images 3, 5 and 7 indicated by arrows) are also shown. Two bridge Hs that desorb from surface are highlighted in red. Two in-plane hydrogen atoms (one in the first tri-layer and the other in the second tri-layer) that diffuse to top of the surface are highlighted in blue. b) Total energy along reaction coordinates. MEP for the same initial state with moment of 0 μ_B and MEP for a degenerated initial state with a magnetic moment of 2 μ_B are included as red dashed line and black dotted lines for comparison. The activation barrier is 1.84 and 1.46 eV, respectively. The square (circle) stands for the state with a magnetic moment of 2 (0) μ_B.

moment of 2 μ_B. The overall kinetic barrier is 1.42 eV. In contrast, without such crossover of magnetic moment, the barrier is 1.46 eV for the same initial state with a magnetic moment of 2 μ_B and 1.84 eV for a degenerated state with a magnetic moment of 2 μ_B.

Our earlier report and also previous studies have shown that the overall desoprtion energy of H (or formation energy) from MgH_2 nanoparticles only decreases significantly when the size of the particle falls below 5 formula units. We have shown via DFT simulation that there is no size effect on the initial desorption of H from a MgH_2 surface and a MgH_2 amorphous nanoparticles. We have considered both singly- and doubly-bonded H. Figure 5(a) shows that a singly-bonded H is removed from an amorphous MgH_2 NP of 31 formula units. The desoprtion energy is 148 kJ/(mol-H_2) in reference to free H_2. Because a singly-bonded H cannot be found on MgH_2(110), where only doubly-bonded H exist, we constructued a stepped surface, see Figure 5(b). The desorption energy of singly-bonded H from this step surface is 140 kJ/(mol-H_2) and within 6% of that from a finite nanoparticle. For a doubly-bonded H, we found a similar result. All the data are shown in Figure 5(c). The lack of size effect in the initial H desorption can be understood by the fact that the Mg-H bond is ionic and local in nature.

Motivated by our earlier STM observations, we used DFT to study the atomic processes of alane formation on Ti-doped Al(111) surfaces and elucidate the role of Ti and vacancies. Figure 6 shows the reaction pathways of alane formation on Al(111) with and without Ti doping. Without Ti (see Figure 6(a)), the pristine Al(111) surface is known to react weakly with hydrogen. The dissociative adsorption

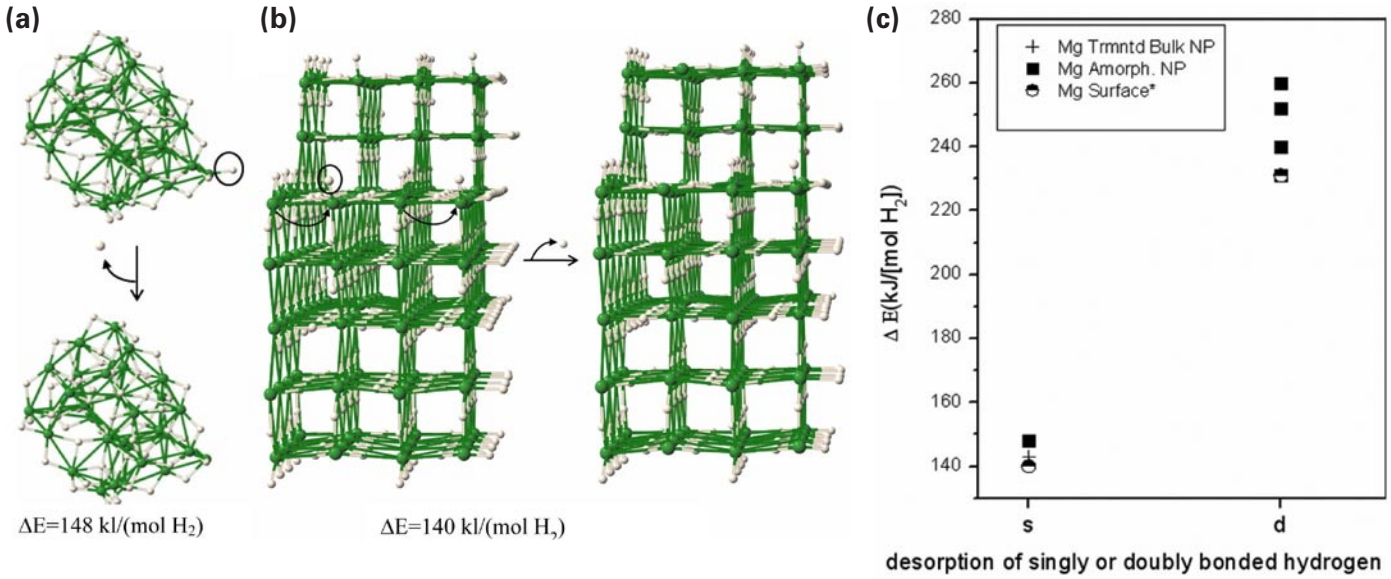

FIGURE 5. Desorption of H from MgH_2 nanoparticle and bulk surface. Singly-bonded H is desorbed from a) an amorphous MgH_2 nanoparticle and b) a stepped surface of MgH_2. c) Desorption energies for both singly- and doubly-bonded H in different structures. In the amorphous MgH_2 nanoparticle, several doubly-bonded H sites that are non-equivalent are shown together.

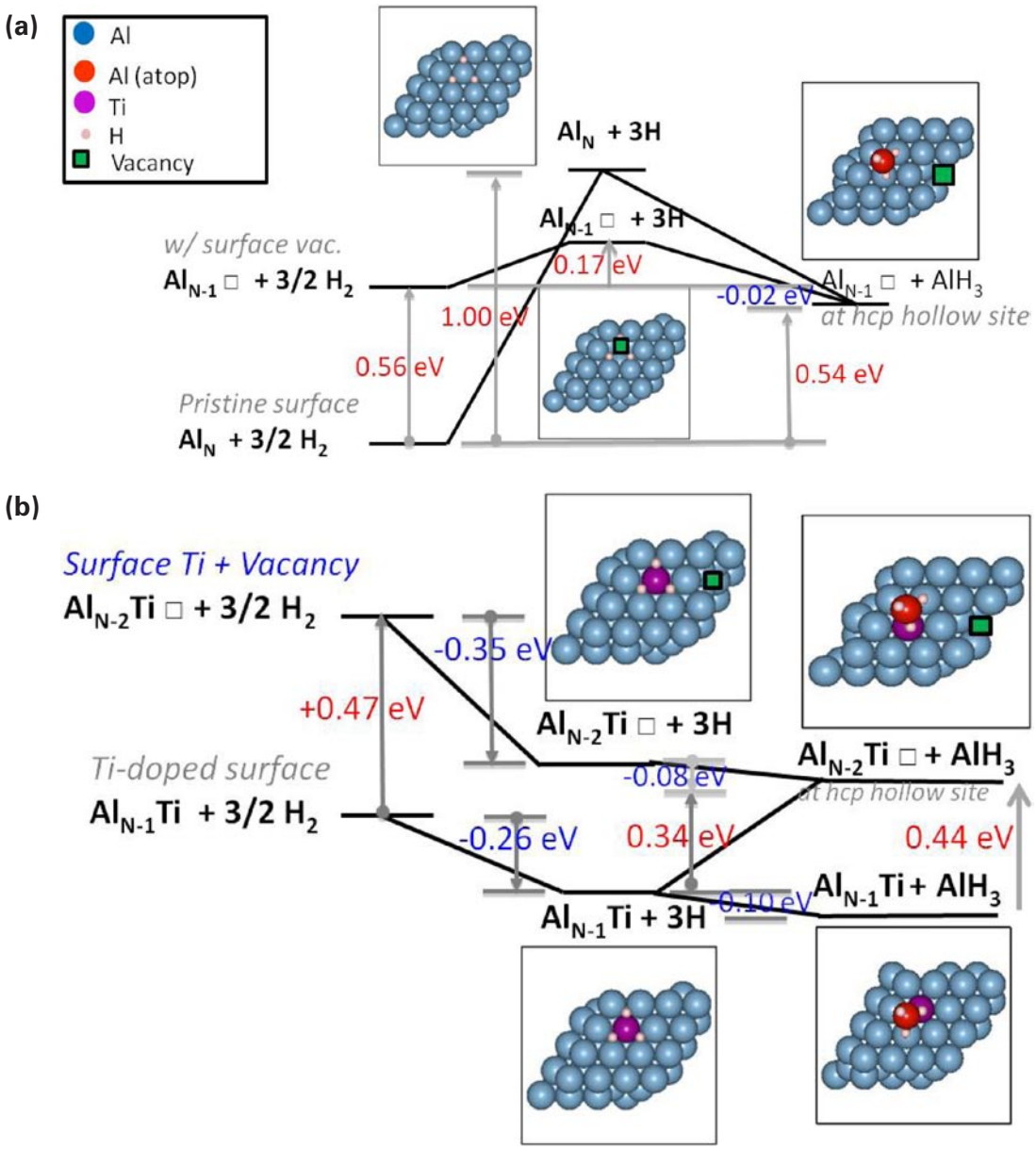

FIGURE 6. Reaction pathways for alane formation on Al(111) (a) without (b) with Ti dopant. In each case, both the absence and presence of Al vacancy are considered.

of H_2 on Al(111) surface costs energy. Using one and a half H_2 molecules and pristine Al(111) surface as the energy reference, the formation of three atomically adsorbed H on Al(111) is 1.00 eV higher. The system can lower energy by 0.46 eV with the formation of an alane molecule, which prefers to adsorb on a neighboring 3-fold hollow site, leaving behind a surface Al vacancy. Overall, the reaction to form alane on pristine Al(111) is endothermic with a reaction energy of 0.54 eV. In contrast, if Al(111) already has an Al vacancy, it only costs 0.17 eV to dissocate (3/2)H_2, which prefers to adsorb at the vacancy site. Then it gains 0.19 eV to form an alane molecule, such that the overall alane formation is slightly exothermic with a reaction energy of -0.02 eV. This is due to the fact that the initial reactant Al phase is destablized by creating one Al vacancy and moving the displaced Al atom to a bulk environment, which shifts the initial state to be 0.56 eV higher. More importantly, the presence of Al vacancy helps to lower the energy cost to dissociate H_2.

By introducing Ti on Al(111) (see Figure 6b), the Al vacancy formation energy is reduced to 0.47 eV, reflecting the tendence for Ti and Al to form an alloy. With Ti, the dissociation of H_2 becomes favored in both cases, with an energy drop of 0.26 and 0.35 eV without and with an Al vacancy, respectively. Atomic H prefers to stay with Ti and adsorbs on the 3-fold hollow site around Ti. Then

the formation of alane is favored by a small energy drop of 0.08 eV in the vacancy case. Without a vacancy, the formation of alane can also proceed with an energy drop of 0.10 eV provided an activated Al atom is available from the creation of a vacancy at another site. Otherwise, a direct conversion to alane by creating a local Al vacancy costs 0.34 eV. But the overall formation of alane in this case with Ti is slightly endothermic with a reaction energy of only 0.08 eV. With the avalability of an activated Al atom diffusing on the surface, the formation of alane molecule in both cases is endothermic. Further study of the kinetic energy barrier of each step is in progress.

Overall, however, these results explain and agree well with our STM studies performed on Al(111) dosed with Ti dopants and H_2; moreover, these results explain the observed formation of alane in ball-milling experiments, where vacancies occur as a inherent consequence of the processing, e.g., those at Ames Laboratory by V. Pacharsky.

Graduate Students and Post-Doctoral Fellows Supported

1. Stephen House, Aditi Herwadkar, Lin-Lin Wang, and Jason Reich

References

1. Majzoub, E.H., X.F. Liu, D. Peaslee, and C.Z. Jost, *Controlling the Decomposition Pathway of LiBH(4) via Confinement in Highly Ordered Nanoporous Carbon.* J Phys Chem C, 2010. 114(33): p. 14036-14041.

FY 2011 Publicatons

1. Location of Ti catalyst in the reversible AlH_3 adduct of triethylenediamine, D.D. Graham, J. Graetz, J. Reilly, J. Wegrzyn, and I.M. Robertson. Journal of Physical Chemistry C, 114, 15207-15211.2010.

2. Time-dependent, protein-directed growth of gold nanoparticles within a single crystal of lysozyme. W. Hui; W. Zidong; Z. Jiong: S. House; G. Yi-Gui; Y. Limin; H. Robinson; T. Li Huey; X. Hang; H. Changjun; I.M. Robertson; Z. Jian-Min; L. Yi. Nature Nanotechnology, 6, 93-97.2011.

3. Ordered metal nanostructure self-assembly using metal–organic frameworks as templates B.W. Jacobs; R.J.T. Houk; M.R. Anstey; S.D. House; I.M. Robertson; A.A. Talin; M.D. Allendorf, Chemical Science, 2, 411-416.2011.

4. Electron Tomographic Characterization of Nano-confined Hydrides for Hydrogen Storage S.D. House, E.H. Majzoub, R. Bhakta, M.D. Allendorf, and I.M. Robertson. Microscopy and Microanalysis conference, 2011.

5. Applications of Electron Microscopy to Complex Metal Hydrides (INVITED) S. House, I.M. Robertson and D. Graham, Microscopy and Microanalysis conference, 2011.

6. Hydrogen Desorption for MgH_2 Surfaces and Nanoparticles: Thermodynamics and Size Effects J. Reich, L.-L. Wang, and D.D. Johnson, in preparation (2011).

7. Kinetic Barriers and Ti-dopant Effects for Hydrogen Desorption on MgH_2(110): a DFT study J. Reich, L.-L. Wang, and D.D. Johnson, in preparation (2011).

8. Defect-mediated Alane Formation in Al(111): DFT comparison to Experiment Aditi Herwadkar, L.-L. Wang, S. House, P Martin, I.M. Robertson, D.D. Johnson, in preparation (2011).

FY 2011 Presentations

1. D.D. Johnson "Quantitative Prediction of Thermodynamic and Mechanical Properties of Real Materials," Invited, International Workshop on Ab-initio Description of Iron and Steel: Mechanical properties (ADIS2010), Ringberg Castle (Tegernsee, Germany) 24–29 October 2010.

2. D.D. Johnson and L-L. Wang, "Nanoparticle Structure and Properties: Universal Features, Structural Instabilities and the Effects of Size and Support", Dept. of Chemical Eng., U. of Pittsburg, 5 November 2010.

3. D.D. Johnson, "Transition-Metal Nanoparticle Structure and Properties: universal features for catalysis," Pennergy Colloquia Series, U. of Pennsylvania, 8 November 2010 (host Andrew Rappe).

4. D.D. Johnson, "Doping and Structural Defects – their import in determining critical materials behavior," Division of Materials Science and Engineering, Ames Laboratory, Iowa State U., 7 December 2010.

5. D.D. Johnson "Disorder-Mediated Quantum Criticality in Laves-phase NbFe2," Department of Physics, 22 February 2011.

6. Aditi Herwadkar and D.D. Johnson, "Defect-mediated Alane formation on Al(111)," 2011 APS March Meeting.

7. Jason Reich, LinLin Wang and D.D. Johnson, "Kinetic Barriers for Hydrogen Desorption for TM (un)doped MgH2(110), " 2011 APS March Meeting.

8. LinLin Wang and D.D. Johnson, "Thermodynamics of MgH2 H-storage materials: nanoparticle size and topological structural effects," 2011 APS March Meeting.

9. S.D. House, E.H. Majzoub, R. Bhakta, M.D. Allendorf, and I.M. Robertson. "Electron Tomographic Characterization of Nano-confined Hydrides for Hydrogen Storage," Microscopy and Microanalysis conference, 2011.

10. S. House, I.M. Robertson and D. Graham, Applications of Electron Microscopy to Complex Metal Hydrides (INVITED) Microscopy and Microanalysis conference, 2011.

11. S.D. House and I.M. Robertson "Microstructural characterization of nano-confined hydrogen storage systems" Gordon research conference, 2011 (INVITED).